Conformational Changes in the Rod Domain of Human Keratin 8 following Heterotypic Association with Keratin 18 and Its Implication for Filament Stability[†]

Ahmad Waseem,[*,‡] Uwe Karsten,[§] Irene M. Leigh,[||] Patricia Purkis,[⊥] Naushin H. Waseem,[@] and E. Birgitte Lane[#]

Programme in Oral Oncology, Oral Diseases Research Centre, Bart's and The London, Queen Mary's School of Medicine and Dentistry, London, U.K., Max Delbruck Centre for Molecular Medicine, Berlin-Buch, Germany, Centre for Cutaneous Research, The Royal London Hospital, London, U.K., The Orchid Cancer Appeal, Williamson Laboratory, St. Bartholomew's Hospital, London, U.K., Department of Molecular Genetics, Institute of Ophthalmology, University College London, London, U.K., and School of Life Sciences, Medical Sciences Institute/Wellcome Trust Building Complex, University of Dundee, Dundee, Scotland

Received June 20, 2003; Revised Manuscript Received October 6, 2003

ABSTRACT: Keratin intermediate filaments are heteropolymers of type I and type II polypeptides that constitute the bulk of the epithelial cytoskeleton. We microinjected seven keratin monoclonal antibodies into human epithelial cells, and two of them, only A45-B/B3 and LP3K, caused the formation of keratin aggregates. The keratin filaments in human epithelial cells were also disrupted by a monovalent A45-B/B3 Fab fragment, suggesting that the binding of the antibody, rather than cross-linking, collapses the filaments. Immunoblotting and ELISA experiments suggested that the antibody reacted weakly with recombinant K8 but did not react with recombinant K18 at all. However, the antibody reactivity increased substantially when a mixture of the two keratin polypeptides, either recombinant or derived from MCF-7, was used. The epitopes of 15 monoclonal antibodies recognizing human K8 were characterized by their reactivity with recombinant fragments of K8. Reactivity of antibody A45-B/B3 with fragments of K8 in the presence of K18 revealed that the antibody recognizes an epitope in the rod domain of K8, between residues 313 and 332, on the amino-terminal side of the stutter in helix 2B, which is involved in heterotypic association. The data suggest that this region of K8 undergoes a conformational change following interaction with the complementary K18 either to expose the epitope or to increase its affinity for the antibody. Taken together, the data highlight the role of this epitope in heterotypic association and in filament stabilization.

The intermediate filaments in epithelia are made of keratins, a family of highly homologous and chemically stable structural proteins. In the human genome database, there are 49 genes for keratins (*1*); of these, 27 genes are expressed in soft epithelia [also termed cytokeratins (*2*)]. A further 15 are expressed in epidermal appendages, such as hair and nails, and are often described as trichocyte or "hard" keratins (*3*, *4*). The remaining seven genes are uncharacterized, and their expression pattern is not known. The entire keratin family is divided into two groups based on gene structure, physicochemical characteristics, and mode of expression; type I keratins are smaller (M_r = 40−56 kDa) and acidic (pI = 4−6) and include K9−K21 and Ha1−Ha8, whereas type II keratins are larger (M_r = 53−67 kDa) and basic or neutral (pI = 6−8) and include K1−K8 and Hb1−Hb6 (*2*, *5*). Keratin filaments are heteropolymers of type I and type II polypeptides, and at least one member of each type is required for filament assembly *in vivo* and *in vitro* (*6*, *7*). Expression of different keratin pairs is tissue- and differentiation-dependent; for example, the keratin K8−K18 pair is expressed in simple and glandular epithelia, and the K5−K14 pair is expressed in basal keratinocytes of stratified epithelia (*2*, *8*) and basal cells in glandular epithelia (*9*).

The secondary structure of intermediate filaments consists of a central rod domain of 310−350 residues flanked by N-terminal head and C-terminal tail domains. The rod domain has four α-helical segments (1A, 1B, 2A, and 2B), each with a heptad repeat, $(abcdefg)_n$, where positions *a* and *d* are generally occupied by apolar residues and the rest are either ionic or charged (*10*). Three non-heptad-containing linkers, L1, L12, and L2, join segments 1A to 1B, 1B to 2A, and 2A to 2B, respectively, thus interrupting the α-helical continuity at three places within the rod domain. Another irregularity within segment 2B, called the "stutter", appears to have been caused by deletion of three consecutive residues or insertion of four residues in an otherwise continuous series of heptad repeats (*11*). These discontinuities perhaps provide added flexibility for polypeptide association during filament assembly, which is an intrinsic feature of these polypeptides. Polymerization of keratin intermediate filaments involves heterotypic association between complementary keratins into elongated dimers, the building blocks

[†] Support for this work came from several sources, including the Wellcome Trust (Grant 055090/C/98Z to I.M.L.), the Cancer Research UK (Grants C26/A1461 and SP2060 to E.B.L.), and the RAB Charitable Foundation of Queen Mary, University of London.

* To whom correspondence should be addressed: Department of Clinical and Diagnostic Oral Sciences, 2 Newark St., London E1 2AT, United Kingdom. Telephone: 0044-20-7882 7138. Fax: 0044-20-7882 7153. E-mail: a.waseem@qmul.ac.uk.

[‡] Queen Mary's School of Medicine and Dentistry.

[§] Max Delbruck Centre for Molecular Medicine.

[||] The Royal London Hospital.

[⊥] St. Bartholomew's Hospital.

[@] University College London.

[#] University of Dundee.

10.1021/bi035072s CCC: $27.50
Published on Web 01/13/2004

of mature filaments, in which the rod domains interact in parallel and in axial register to form polar coiled coils (*7*, *12*). In this arrangement, the hydrophobic *a* and *d* position residues alternate along the interaction plane between the two α-helices in an extended "leucine zipper" configuration, and are sequestered from the aqueous cytoplasm. Cross-linking and *in vitro* assembly experiments in intermediate filaments have shown that dimers then associate in an antiparallel manner in four modes of association, one in register, two staggered, and one head to tail, into rate-limiting oligomers (*13*−*16*). These oligomers act as nuclei for polymerization into intermediates before developing into mature filaments (*17*, *18*). Unlike microfilaments and microtubules, the assembled filaments are nonpolar, and both ends are similar, a characteristic that can be attributed to the antiparallel alignment of polar dimers.

Despite their mechanical stability and extremely low solubility, there is a large body of data to suggest that intermediate filaments, including keratins, are dynamic structures *in vivo*. Thus, disruption and reassembly of intermediate filaments during mitosis (*19*−*21*), integration of keratins expressed from microinjected mRNA (*22*, *23*) or from transfected plasmids, and disruption of the preexisting keratin network by truncated polypeptide (*24*, *25*) have all given clues suggesting their dynamic nature. Rapid exchange of intermediate filament subunits as observed by microinjection of biotinylated keratins (*26*, *27*), fluorescence recovery after photobleaching using Xrhodamine-labeled filament proteins (*28*, *29*), and experiments using fluorescence resonance energy transfer (*30*) support the existence of an equilibrium between the soluble pool of protein subunits and the polymerized filaments. This exchange of subunits perhaps allows the filaments to reorganize in response to extracellular stimuli, including heat shock and growth factors (*31*, *32*). Integration of single keratins into the preexisting network may also suggest the existence of multiple equilibria for creation of a small pool of single keratins that are able to form heterotypic complexes with the microinjected or transfected keratins. The exchange of keratin oligomers in the soluble pool with keratin filaments involves high-affinity sites created by the association and subsequent folding of the polypeptides. These sites can be identified using synthetic peptides, which not only inhibit polymerization but also solubilize preformed filaments by blocking these associations *in vitro* and *in vivo* (*14*, *15*, *33*−*35*).

Monoclonal antibodies with defined specificity and well-characterized epitopes have also been used for structural analysis of intermediate filaments (*36*, *37*). Microinjection of some antibodies disrupts the preexisting keratin filament network (*33*, *38*−*41*), suggesting that the antibody binding regions might be part of the high-affinity association sites essential for filament stability. In this study, we have microinjected seven different anti-keratin monoclonal antibodies into epithelial cells in culture and observed extensive filament disruption caused by two antibodies, LP3K and A45-B/B3. We then mapped the epitopes of these and eight other monoclonals to K8 using expressed fragments of the K8 polypeptide. Epitope analysis showed that LP3K maps close to the end of coil 2B, a region known to play a vital role in filament stabilization (*33*−*35*, *42*, *43*). The A45-B/B3 antibody reacts with the rod domain of K8, but the reactivity increases with a mixture of keratins K8 and K18. This antibody can thus distinguish between the K8 in homodimers and the K8 which is part of the heterotypic complex with K18. Our data suggest that the region recognized by the A45-B/B3 antibody undergoes a conformational change following association with K18 and plays an important role in filament assembly and/or stability.

Table 1: Monoclonal Anti-Cytokeratin Antibodies Used in Epitope Analysis

monoclonal antibody	reported specificity
LE41 (*73*)	K8
M20 (*74*)	K8
NCL-5D3 (*75*)	K8
C43 (*76*)	K8
TS 1 (*77*)	K8
C22 (*76*)	K5, K8
TROMA1 (*78*)	K8
CAM5.2 (*61*)	K8, K18, K19[a]
TS 3 (*77*)	K7, K8
TS 7 (*77*)	K7, K8
LP3K (*79*)	K7, K8
RCK102 (*80*)	K5, K8
A45-B/B3 (*54*)	K1, K2, K5, K8, K18
KG8.13 (*81*)	K1, K5, K6, K7, K8, K10, K18
AE3 (*82*)	K1, K2, K3, K4, K5, K6, K7, K8
RCK105 (*83*)	K7
RCK106 (*84*)	K18
anti-IFA (*69*)	all intermediate filaments

[a] Although CAM5.2 has been reported to recognize K8, K18, and K19, subsequent studies suggested that it does not react with K18 and K19 but recognizes K7 and K8 (*62*).

EXPERIMENTAL PROCEDURES

Materials. The monoclonal antibodies used in this study and their reported specificities are listed in Table 1. The antibodies KG8.13 (Sigma) and NCL-5D3 (Novocastra) were obtained commercially. Other antibodies used in this study were donated by colleagues as tissue culture supernatants: TROMA1 from R. Kemler (Department of Molecular Embryology, Max-Planck Institute of Immunobiology, Freiburg, Germany), M20 and RCK102 from F. C. S. Ramaekers (Department of Molecular Cell Biology, University of Maastricht, Maastricht, The Netherlands), C22 and C43 from J. Kovarik (Masaryk Memorial Cancer Institute, Brno, Czech Republic), and TS 1, TS 3, and TS 7 from T. Stigbrand (University of Umeå, Umeå, Sweden). Purified AE3 and CAM5.2 were provided by M. Klymkowsky (University of Colorado, Boulder, CO) and by C. Dixon (Cancer Research UK), respectively. Purified antibody BG2, raised against bacterial β-galactosidase, was provided by D. Lane (Department of Surgery and Molecular Oncology, University of Dundee). Antibodies A45-B/B3, anti-IFA, LP3K, and LE41 were obtained by culturing the respective hybridomas.

Cell Culture. The following epithelial cell lines were used in this study: MCF-7 and BT20 (human breast cancer cell lines), HeLa (human cervical adenocarcinoma), TR146 (human oral squamous cell carcinoma), and PtK2 (rat kangaroo kidney epithelia). All cells were cultured in Dulbecco's modified Eagle's medium (DMEM) containing

Table 2: Nucleotide Sequences of Primers in Reverse Orientation Used in the PCR Amplification of K8 cDNA Fragments

GST-K8 fragment	nucleotide sequence,[a] from 5′ to 3′	size of the K8 fragments (amino acids)
K8CΔ151	ATCTGCGGATCC*TTA*CTCCAGGGAAGCCCTCTG	1−332
K8CΔ161	CTGGCCGGATCC*TTA*CTCAATCTCAGCCTGGAG	1−322
K8CΔ171	GAGCCGGGATCC*TTA*CCGGTTCATCTCAGAGAT	1−312
K8CΔ417	GCTCTGGGATCC*TTA*AACTGCGGTGATGCC	1−66

[a] A *Bam*HI restriction site inserted in all reverse primers is underlined. The three nucleotides inserted to introduce a stop codon into the sense strand (here TTA) are in italics.

10% (v/v) fetal calf serum (FCS) and maintained at 37 °C in a humidified atmosphere of 5% CO_2 and 95% air. Hybridoma cells producing LP3K, LE41, anti-IFA, and A45-B/B3 antibodies were also cultured under similar conditions except that the FCS concentration was 5% (v/v). Ascites fluid was developed by injecting $6-10 \times 10^6$ growing hybridomas in 0.5 mL of PBS into the peritoneum of mice previously primed with pristane. The ascites fluid was collected from the peritoneum after approximately 1 week and used for antibody purification.

Purification of Monoclonal Antibodies. Antibodies were purified from culture supernatant or from ascites fluid on an Affi-Prep protein A column (Bio-Rad) as described previously (*44*). Briefly, the antibodies were precipitated using ammonium sulfate, and a concentrated solution was loaded onto an Affi-Prep protein A column equilibrated with a high-salt solution. The antibodies of different IgG subclasses were eluted from the column in 100 mM citrate buffer at pH 6.0 for IgG1 (A45-B/B3, LE41, M20, RCK102, and anti-IFA), pH 5.0 for IgG2a (NCL-5D3 and CAM5.2), and pH 4.0 for IgG2b (LP3K), immediately neutralized with 1 M Tris base, dialyzed, and stored in aliquots at −20 °C. The protein A column was regenerated with 50% (v/v) methanol and washed with 0.5 M sodium hydroxide between runs to prevent cross contamination. When ascites fluid was used for antibody purification, the ammonium sulfate precipitation step was omitted. Sodium chloride and borate concentrations were adjusted, and purification was carried out as described previously (*44*). The monovalent Fab fragment of the A45-B/B3 monoclonal antibody was prepared by proteolytic cleavage with papain as described elsewhere (*45*).

Microinjection. The antibody or monovalent Fab preparations were first dialyzed extensively against injection buffer I [114 mM KCl, 14 mM NaCl, 3 mM $MgCl_2$, and 3 mM Na_2HPO_4 (pH 7.0)] (*46*) or II [50 mM NaCl and 10 mM Tris-HCl (pH 7.6)] and concentrated using a Centricon 10 ultrafiltration device (Millipore) to a protein concentration of 3−40 mg/mL. The epithelial cells were seeded on plastic tissue culture dishes (5 cm in diameter) at 5−10% confluence and were grown for 1−2 days. Just before the experiment, the cells were washed with DMEM without FCS and the microinjection was carried out using an inverted microscope (Zeiss) equipped with a heated stage and long working distance lenses. The antibody solution was injected into epithelial cells using a glass microcapillary needle controlled by a micromanipulator (Eppendorf). During microinjection, the cells were kept at 37 °C in an open atmosphere and the pH of the medium was maintained with 0.1 M HEPES (pH 7.4). There was no detectable influence on the cell shape during or after microinjection except the predictable swelling of membrane, which disappeared after a few hours. The intercellular contacts also remained unaffected by the microinjection. The high degree of cell survival (60−70%) following microinjection also suggested that their ability to attach remained intact.

Approximately 40−50 cells were injected at a time in a tissue culture dish, and each set was repeated at least three times often on different dates to test the reproducibility. Four different epithelial cell lines (BT20, MCF-7, TR146, and PtK2) were used for microinjection. Approximately 70% of the cells which survived the microinjection and remained attached to the culture dish were identified by staining with fluorescein isothiocynate (FITC)-labeled goat anti-mouse antibody.

Cloning and Manipulation of Keratin K8 and K18 cDNAs. Full-length K8 and K18 cDNAs were subcloned into the *Eco*RI site of pUCR1, and the proteins expressed using these constructs were termed PUC-K8 and PUC-K18, respectively, as described previously (*44*, *47*). Keratin K8 fragments were generated by PCR to produce a series of 14 fragments progressively deleted from the C-terminus. These were prepared as glutathione *S*-transferase (GST) fusion proteins by subcloning the K8 cDNA fragments, amplified by the PCR, into pGEX-2TE (*44*). The forward and reverse oligonucleotides used in the PCR amplification of 10 K8 fragments have been described previously (*44*). The sequences of reverse primers used in the preparation of four additional fragments (K8CΔ151, K8CΔ161, K8CΔ171, and K8CΔ417) are listed in Table 2. The same forward primer with a unique *Eco*RI cloning site was employed in all amplifications to keep the N-terminus sequence identical to the wild-type K8 sequence in all fragments. The reverse primers were constructed to introduce a stop codon just after the unique *Bam*HI site in the sense strand (see Table 2). After a double digestion with *Eco*RI and *Bam*HI, all K8 fragments were ligated into the corresponding sites of pGEX-2TE and confirmed by sequencing. One of the K8 fragments, K8Δ80, was also subcloned into *Eco*RI and *Bam*HI sites of pMap1, a vector derived from pUR292 (*48*), to produce a β-galactosidase fusion protein. The pGEX and pMap constructs were introduced into *Escherichia coli* strain DH5-α (Invitrogen) or recombination deficient Sure cells (Stratagene), and the transformants were used for protein expression. All constructs were named starting with the expression plasmid followed by K8 and C*Δ*X*, where *X* was the number of residues deleted from the C-terminus. The fusion proteins were named similarly except that the plasmid names were replaced with GST or β-gal (see Table 2 and Figure 9).

Expression and Purification of the Fusion Proteins. Overnight cultures of the recombinant bacteria were diluted to an optical density of 0.5 at 600 nm. The cultures were then induced to express the keratin fusion proteins by adding 500 μM isopropyl thio-β-D-galactopyranoside and allowed to grow for 3 h. The bacteria from 3 mL cultures were

pelleted and suspended in 100 μL of 3× SDS sample buffer [60 mM Tris-HCl (pH 8.0), 300 mM dithiothreitol, 4.5% SDS, and 30% glycerol], incubated in a boiling water bath for 10 min, and stored in aliquots at −20 °C. The samples were diluted 3-fold with water before being run on a 12% SDS−polyacrylamide gel electrophoresis (SDS−PAGE) gel and staining with Coomassie brilliant blue. The fusion proteins were identified by comparing the SDS−PAGE profile of bacteria containing the constructs with those of the vector alone.

For immunodetection, the keratin polypeptides separated on SDS gels were electrophoretically transferred onto nitrocellulose membranes. The membranes were blocked with 3−10% (w/v) nonfat milk or 0.5−10% BSA in PBS for 1 h followed by incubation for 1 h with the primary antibody diluted 1:5 in expired DMEM and 10% FCS. After being washed with water for 2 min, the membranes were incubated with alkaline phosphatase-labeled goat anti-mouse IgG (DAKO) at a dilution of 1:500 in DMEM and FCS for 1 h. The membranes were washed as described above, and the bound antibody was detected using a mixture of nitro blue tetrazolium and 5-bromo-4-chloro-3-indolyl phosphate (NBT/BCIP) as the substrate for alkaline phosphatase (*44*).

Purification of full-length K8 and K18 from recombinant bacteria was carried out as described previously (*44*) except that gel filtration in the presence of guanidine hydrochloride was omitted. The chimeric protein β-gal-K8Δ80 containing the entire head and rod domains was prepared from recombinant *E. coli*. The inclusion bodies were washed twice in 2 M urea, dissolved in 8 M urea in 20 mM Tris-HCl buffer (pH 8.0), and cleared by high-speed centrifugation. This fragment was purified on a single-stranded DNA−agarose column (Sigma) in 6 M urea (*7*).

Keratin polypeptides from MCF-7 cells were extracted following the procedure described previously (*44*). SDS−PAGE analysis showed three protein bands corresponding to 58 (K8), 49 (K18), and 40 kDa (K19).

Enzyme-Linked Immunosorbent Assay (ELISA). Recombinant keratins or the detergent insoluble extract of MCF-7 was dissolved in 8 M urea or 4 M guanidinium hydrochloride, and after the residual insoluble material had been removed with a high-speed spin, the supernatant was diluted with 100 mM sodium bicarbonate buffer (pH 9.6) to a final protein concentration of ∼20 μg/mL and a denaturant concentration of less than 100 mM. This solution was then used to coat 96-well ELISA plates overnight at 4 °C. After being blocked with 100 μg/mL BSA in PBS (BSA/PBS) for 2−3 h at room temperature, the plates were incubated with primary antibodies serially diluted in BSA/PBS. For competition ELISA assays, the competing antibody (or Fab) was mixed with the biotinylated antibody and incubated in the antigen-coated wells. After being washed with 0.05% Tween 20 in PBS, the plates were incubated with peroxidase-conjugated rabbit anti-mouse IgG. The bound peroxidase activity was detected with *o*-phenylenediamine hydrochloride and hydrogen peroxide, and the color was read at 495 nm in an ELISA reader. In cases where the monoclonal antibodies were biotinylated, peroxidase-conjugated streptavidin was used to detect the bound primary antibody.

Immunofluorescence. Indirect immunofluorescence was performed using the antibody culture supernatant and a goat anti-mouse IgG conjugated with FITC or with Texas red (TR). The cells were washed with PBS and fixed with a mixture of acetone and methanol (1:1). The incubation with a primary and FITC or TR-labeled secondary antibody was carried out as described previously (*49*). The stained cells were overlaid with glass cover slips on 90% glycerol in PBS containing 25 mg/mL 1,4-diazabicyclo(2,2,2)octane as an antifading agent. The fluorescence was viewed in an immunofluorescence microscope and photographed using TMAX-3200 film (Kodak).

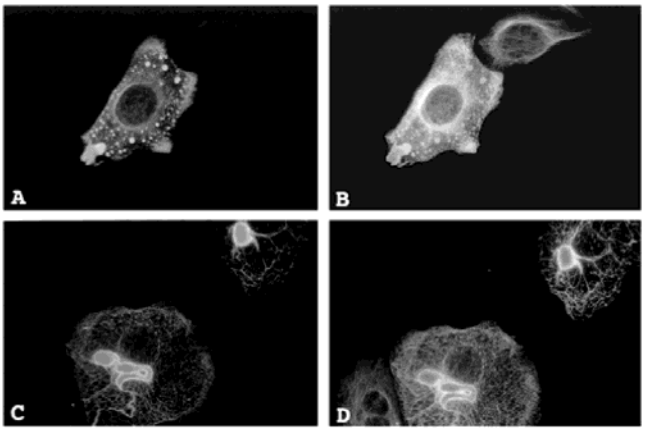

FIGURE 1: Microinjection of A45-B/B3 into MCF-7 cells. MCF-7 cells were plated at 5−10% confluence at least 24 h before microinjection. Affinity-purified A45-B/B3 (7 mg/mL) in injection buffer I was microinjected using a microcapillary needle as described above. The cells were fixed in a mixture of methanol and acetone (1:1) and stained with FITC-labeled goat anti-mouse antibody. The cells were further incubated with RCK106, an anti-K18 antibody, washed, and counterstained with TR-labeled goat anti-mouse antibody. The cells were visualized under a fluorescence microscope: (A and C) FITC and (B and D) TR. The pattern of filament disruption in panels A and B is different from that in panels C and D.

The microinjected cells were also processed for immunofluorescence as described above except that the incubation step with the primary antibody was omitted and instead the cells were directly treated with FITC-labeled goat anti-mouse antibody (*39*). This allowed unambiguous identification of a bright green injected cell in a field of uninjected controls. To compare the injected cells with the uninjected controls in the same dish, the cells were stained for double immunofluorescence with a second keratin antibody (LE41, RCK106, or RCK105) and then counterstained with TR-labeled goat anti-mouse antibody (Figures 1 and 5).

Other Methods. Amplification of K8 cDNA fragments was carried out by PCR using the high-fidelity thermostable Pwo DNA polymerase from *Pyrococcus woesei* (Roche) as described previously (*44*). DNA constructs were sequenced using the Big Dye sequencing reaction kit and analyzed on an ABI Prism 377 sequencer (Applied Biosystems). Routine purification of DNA fragments, their phosphorylation and ligation, was carried out using standard procedures (*50*). The protein concentration of an IgG solution was determined at 280 nm using an $E_{1\%}$ of 13.75. The protein concentration in dilute keratin solutions was determined using the dye binding Bradford assay (*51*). Biotinylation of affinity-purified antibodies was carried out using biotin *N*-hydroxysuccinimide as described elsewhere (*45*).

All gel pictures and immunofluorescence slides were scanned and assembled on a PowerMac using Photoshop version 7.

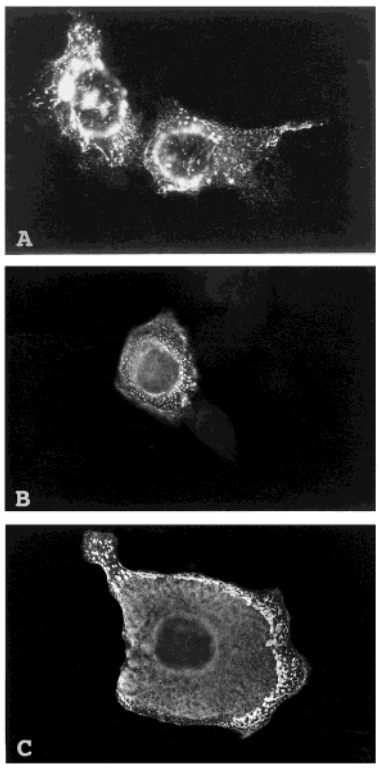

FIGURE 2: Microinjection of A45-B/B3 into epithelial cells. Three epithelial cell lines, (A) HeLa, (B) TR146, and (C) BT20, were plated at 5−10% confluence 24 h before microinjection of 6 mg/mL affinity-purified A45-B/B3. Cells were left to recover overnight at 37 °C before being fixed in a mixture of acetone and methanol (1:1), stained with FITC-labeled goat anti-mouse antibody, and visualized by fluorescence microscopy.

RESULTS

Disruption of Keratin Filaments by Microinjection of A45-B/B3. Microinjection of 8−10 mg/mL A45-B/B3 into MCF-7 cells produced punctate (globular) staining when the cells were examined 16 h later with FITC-labeled goat anti-mouse antibody (Figure 1A,B). These aggregates could be counterstained with RCK106, specific for K18, or LE41, specific for K8, and TR-labeled goat anti-mouse antibody. In some cells, the filaments collapsed and formed a large aggregate on one side of the nucleus (Figure 1C,D). The collapse of keratin filaments was apparent at ∼3 mg/mL, the lowest concentration used in this study. In BT20 and HeLa, both simple epithelial cell lines, and TR146, a keratinocyte cell line, we observed extensive filament disruption similar to that seen in MCF-7 cells (Figure 2). The filament disruption was independent of the keratin antibody used for counterstaining. For example, similar patterns were observed whether injected HeLa cells were counterstained with RCK106 (anti-K18) or RCK105 (anti-K7) (not shown).

We microinjected seven other antibodies into MCF-7 cells, and of these, only one other, LP3K, was also able to disrupt filaments (Figure 3C). We observed no filament collapse following microinjection of NCL-5D3 (Figure 3A,D), but the filaments appeared to be thin and showed a loss of bundling of keratin filaments, similar to results observed on microinjection of LE41 (*39*). Increasing the antibody concentrations from 5 to 40 mg/mL, using injection buffer I or II, or increasing the time of incubation after microinjection from 2 to 24 h did not change the staining pattern. Microinjection of other antibodies, including LE41, AE3, CAM5.2, RCK102, and M20, in epithelial cell lines, including BT20, PtK2, or MCF-7, produced minor changes in filament organization without complete disruption (Figure 3).

The specificity of the effect of the anti-keratin antibody was investigated by microinjection of BG2, an antibody raised against bacterial β-galactosidase. This antibody produced only a diffuse staining throughout the cytoplasm with no specific staining of keratin filaments (not shown).

Binding of A45-B/B3 Was Sufficient for Filament Disruption. To show that the filament disruption was only due to binding of A45-B/B3 rather than cross-linking of filaments by the bivalent antibody, we prepared a monovalent Fab fragment. This fragment was prepared by papain digestion

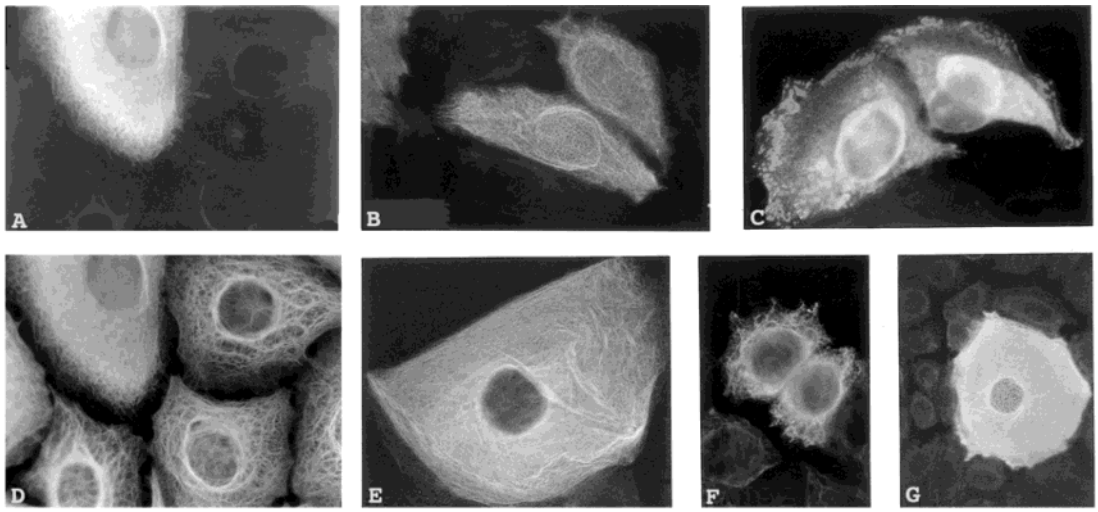

FIGURE 3: Microinjection of anti-keratin antibodies into MCF-7 cells. All antibodies used for microinjection were affinity-purified on a protein A column and equilibrated with injection buffer I. MCF-7 cells were seeded at 5−10% confluence at least 16 h before microinjection of a 10 mg/mL solution. After injection, the cells were left to recover overnight before being fixed in a mixture of acetone and methanol (1:1). The cells were stained with FITC-labeled goat anti-mouse antibody and visualized by immunofluorescence microscopy (A−C and E−G). In some cases, the cells were then counterstained with LE41 and after washing counterstained with TR-labeled goat anti-mouse antibody (D): (A and D) NCL-5D3, (B) LE41, (C) LP3K, (E) RCK102, (F) CAM5.2, and (G) M20.

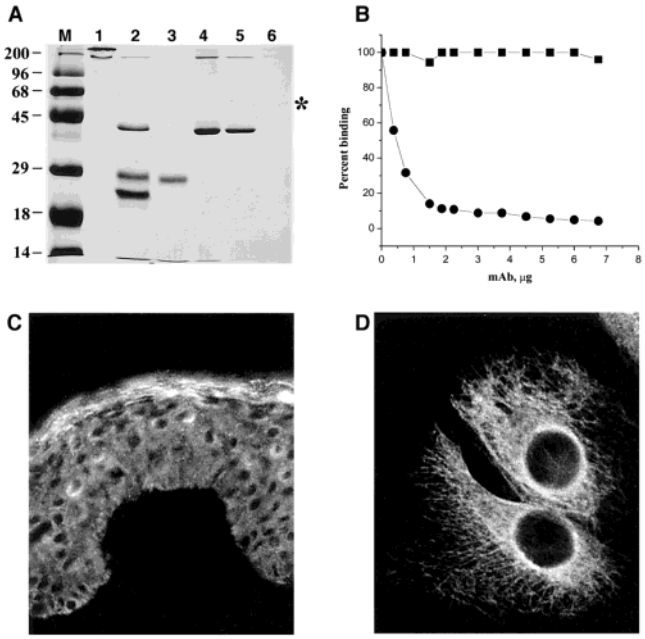

FIGURE 4: Purification and characterization of A45-B/B3 Fab. (A) SDS profile of fractions at various stages of the Fab purification. Thirty-five milligrams of purified A45-B/B3 in 20 mL of 100 mM sodium acetate buffer (pH 5.5) containing 1 mM EDTA and 15 mM cysteine was treated with 175 μg of papain for 7 h at 37 °C. The reaction was terminated by incubating the mixture with 78 mg of iodoacetamide for 2 h. The reaction mixture was applied to a 2 mL protein G column equilibrated in 100 mM Tris-HCl buffer (pH 8.0). The bound protein was eluted with 0.1 M HCl and, after neutralization, eluted through a 2 mL protein A column in high-salt buffer (*44*), and the flow through containing Fab was collected. Samples equivalent to 8 μg of protein were analyzed via 12% SDS−PAGE and visualized with Coomassie brilliant blue: lane 1, undigested A45-B/B3; lane 2, A45-B/B3 digested with papain; lane 3, flow-through from the protein G column; lane 4, protein eluted from the protein G column; lane 5, flow-through from the protein A column; lane 6, protein eluted from the protein A column; and lane M, molecular mass standards myosin (M_r = 200 000 Da), phosphorylase (M_r = 96 000 Da), bovine serum albumin (M_r = 68 000 Da), ovalbumin (M_r = 45 000 Da), carbonic anhydrase (M_r = 29 000 Da), β-lactalbumin (M_r = 18 000 Da), and lysozyme (M_r = 14 000 Da). The absence of heavy (H) and light (L) chains in lane 1 and the presence of a single 43−44 kDa band in lanes 4 and 5 indicated a lack of disulfide bond reduction during SDS sample preparation as described previously (*45*). A faint protein band with an M_r of 54 kDa denoted with an asterisk was eluted from protein G (lane 4) but was removed on the protein A column (lanes 5 and 6). The identity of the high-molecular mass band close to the origin in lanes 4 and 5 was not known, but it was not undigested IgG as it was not retained on the protein A column. (B) Competitive inhibition of A45-B/B3 binding to MCF-7 keratins by LE41 (■) and the A45-B/B3 Fab (●). Keratins extracted from MCF-7 cells were adsorbed on an ELISA plate and incubated with a mixture of biotinylated A45-B/B3 (0.5 μg) and various amounts of either LE41 or A45-B/B3 Fab for 4 h, and the bound biotinylated antibody was detected using peroxidase-labeled streptavidin as described in Experimental Procedures. LE41 does not compete with the A45-B/B3 Fab fragment because its epitope is located closer to the head domain (see Figure 11A). The reactivity of A45-B/B3 Fab with (C) an unfixed frozen section of human skin and (D) keratin filaments in BT20 cells was tested by immunofluorescence using FITC-conjugated secondary antibody; no difference in reactivity was detected.

and purified on protein G and protein A columns (Figure 4A). The Fab was characterized by a competitive ELISA with biotinylated A45-B/B3 for binding to MCF-7 keratins (Figure 4B). A45-B/B3 also reacts with K1 and K5 (see Table 1), and immunostaining of the human epidermis and BT20 cells with the Fab fragment was indistinguishable from that observed with the intact A45-B/B3 (Figure 4C,D).

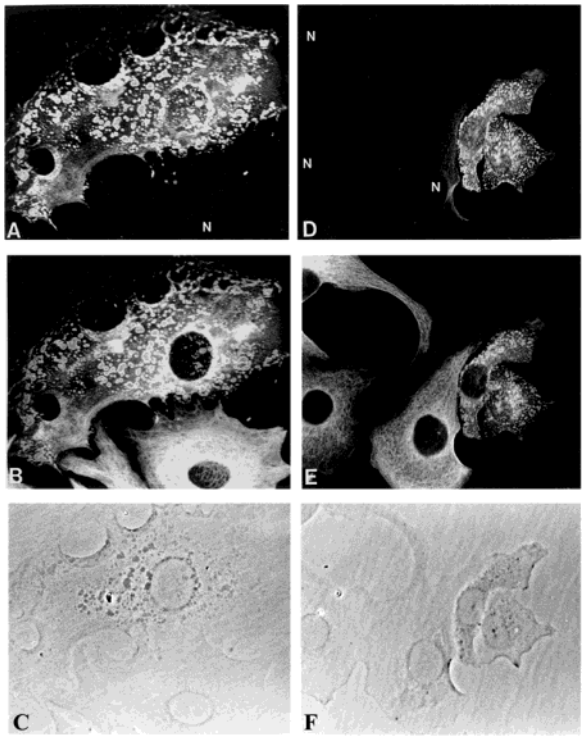

FIGURE 5: Microinjection of A45-B/B3 Fab. Affinity-purified A45-B/B3 Fab (4.5 mg/mL) in buffer I was microinjected into MCF-7 cells (A−C) and BT20 Cells (D−F) as described in the Experimental Procedures. After 18 h, the cells were fixed in methanol and acetone (1:1) and stained with FITC-labeled goat anti-mouse antibody. The cells were further incubated with RCK106 and after washing counterstained with TR-labeled goat anti-mouse antibody and visualized under a fluorescence microscope. (A and D) FITC-stained cells to show A45-B/B3 Fab. (B and E) TR-labeled cells to show all keratin. (C and F) Keratin aggregates are visible as dark bodies in the cytoplasm by phase contrast microscopy. The letter N marks the location of nuclei of control cells in panels A and D.

Approximately 18 h after microinjection of the Fab into MCF-7, keratin filaments could not be detected with the FITC-labeled goat anti-mouse antibody; instead, large globules were seen throughout the cytoplasm (Figure 5A). These aggregates were also visible in phase contrast images of the microinjected cells (compare panels A and C of Figure 5). Counterstaining the cells with RCK106 followed by TR-labeled anti-mouse antibody produced an identical globular pattern (compare panels A and B of Figure 4). Similar observations were made when Fab was microinjected into BT20 cells (Figure 4D−F).

To demonstrate that binding of A45-B/B3 to keratin filaments was necessary for filament disruption, we microinjected the Fab into PtK2 cells, which express the marsupial homologue of human K8, K18, and K19. Although we observed filament disruption in PtK2 by microinjection of LE61 as reported previously (*39*, *52*), microinjection of A45-B/B3 or its Fab fragment did not disrupt keratin filaments in this cell line (not shown). This was due to poor binding of the antibody or its Fab to keratin filaments, since A45-B/B3 stained filaments only weakly in this cell line (not shown). Taken together, the data suggest that binding of antibody was essential for filament disruption.

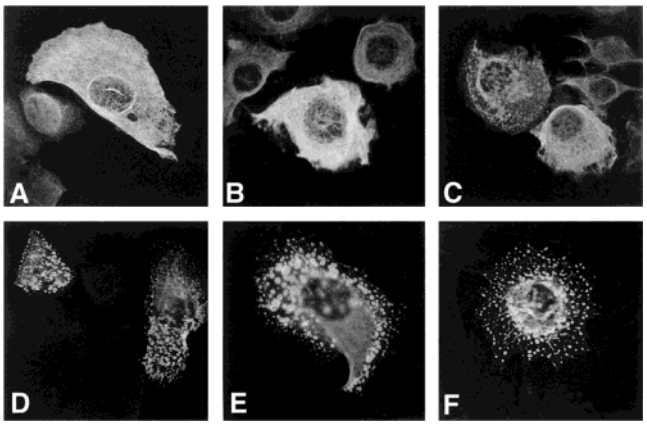

FIGURE 6: Time course of filament disruption in MCF-7 cells by A45-B/B3 Fab. MCF-7 cells were grown for at least 24 h in normal medium and transferred into HEPES-containing medium just before microinjection. Affinity-purified A45-B/B3 Fab (4.5 mg/mL) in injection buffer I was microinjected into MCF-7 cells, fixed with acetone and methanol (1:1) at different time intervals, and stained with FITC-labeled goat anti-mouse antibody. The cells were visualized in a fluorescence microscope: (A) 2 min, (B) 5 min, (C) 10 min, (D) 15 min, (E) 8 h, and (F) 16 h.

Time Course of A45-B/B3-Induced Keratin Filament Disruption. To evaluate the time course of filament disruption, we microinjected 4−6 mg/mL Fab into MCF-7 cells, fixed the cells at different time intervals, and stained the cells with FITC-labeled goat anti-mouse antibody. Two and five minutes after microinjection, the Fab stained keratin filaments with no obvious sign of filament collapse. However, at 10 min the keratin filaments had begun to reorganize; at 15 min complete disruption was achieved with keratin aggregates spread throughout the cytoplasm, and the pattern remained unchanged until 24 h, the latest time point that was examined (Figure 6).

A45-B/B3 Shows Higher Affinity for Keratin Complex than for Recombinant K8. Although A45-B/B3 reacted strongly with keratins as determined by immunofluorescence in tissue sections and cultured cells, it showed only weak reactivity with recombinant K8 and no reactivity with K18 on Western blots. In fact, it was necessary to limit the membrane blocking to only 0.5−1% BSA in PBS to detect binding to K8, as more stringent blocking with 5−10% nonfat milk abrogated any binding (not shown). This prompted us to compare the antibody binding to β-gal-K8Δ80, a K8 fragment containing the head and rod domains with the MCF-7 keratins (including K8, K18, and K19). Binding of four biotinylated antibodies (A45-B/B3, CAM5.2, RCK102, and LP3K) to the recombinant β-gal-K8Δ80 and to MCF-7 keratins was assessed with an ELISA as described in Experimental Procedures. The binding of LP3K and CAM5.2 to the recombinant fragment was almost identical to their binding to MCF-7 keratins (Figure 7). However, RCK102 exhibited a more than 6-fold increase in the level of binding to the MCF-7 extract compared with that for the β-gal-K8Δ80 fragment, and the level of binding of A45-B/B3 to the MCF-7 extract was more than 13-fold higher than that for the K8 fragment. This indicated that RCK102 and A45-B/B3 both had higher affinity for keratin complexes than for the individual K8.

To demonstrate that the level of binding of A45-B/B3 to keratin K8 increases when it forms a complex with K18,

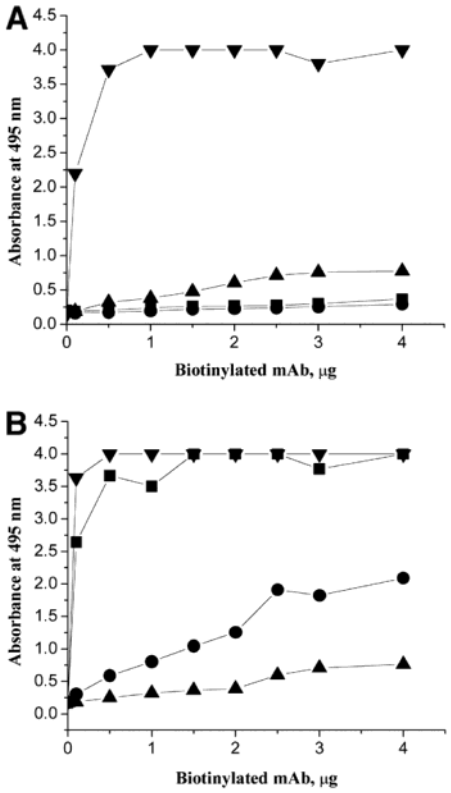

FIGURE 7: Binding of antibodies to βgal-K8Δ80 and MCF-7 keratin complexes. (A) Recombinant βgal-K8Δ80 or (B) keratin complexes isolated from MCF-7 cells were adsorbed to ELISA plates and incubated with biotinylated CAM5.2 (▼), A45-B/B3 (■), RCK102 (●), and LP3K (▲) in BSA/PBS overnight at 4 °C. The bound antibodies were quantified using peroxidase-labeled streptavidin as described in Experimental Procedures. Error bars were deleted for the sake of clarity, but the maximum variation in reactivity was within 10%.

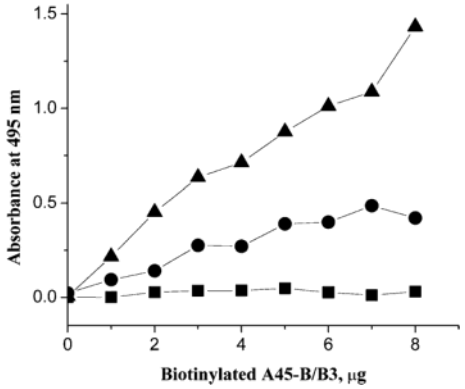

FIGURE 8: Binding of keratin polypeptides and their complexes with A45-B/B3. Samples of purified PUC-K18 (■), PUC-K8 (●), and an equimolar mixture (▲) of the two polypeptides were adsorbed on ELISA plates. The wells were then incubated with different concentrations of biotinylated A45-B/B3, and the bound antibody was detected as described in Experimental Procedures.

we compared binding of the biotinylated A45-B/B3 with individual PUC-K8, PUC-K18, and a mixture of the two polypeptides with an ELISA. No reactivity of A45-B/B3 with PUC-K18 was detected in this assay, but the antibody exhibited significant binding to PUC-K8 (Figure 8). However, the level of antibody binding increased by more than 2-fold when a mixture of the two polypeptides was used in the ELISA. This observation again indicated clearly that

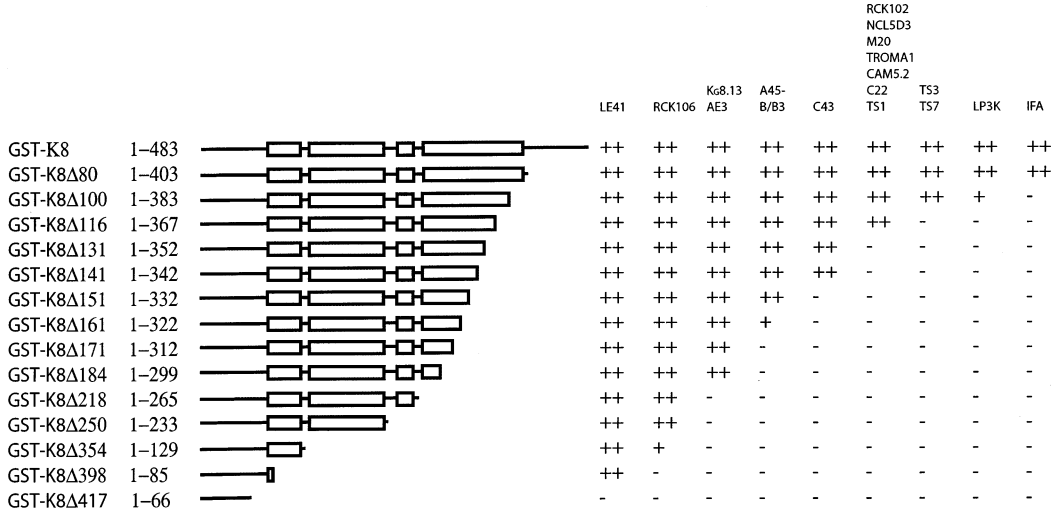

FIGURE 9: Schematic representation of K8 deletion fragments. The secondary structure of K8 with a central α-helix-rich rod domain flanked by nonhelical head and tail domains is shown at the top. The rod domain contains four α-helical subdomains, 1A, 1B, 2A, and 2B (shown in boxes), interspaced by linkers L1, L12, and L2. The 14 fragments were prepared by cloning K8 cDNA fragments with selected PCR primers as described in Experimental Procedures. The deletion mutants are described as K8CΔ*X*, where *X* is the number of amino acids omitted from the carboxy terminus of K8. The reactivity of different fragments with antibodies LE41, A45-B/B3 RCK106, KG8.13, AE3, C43, NCL-5D3, M20, TROMA1, CAM5.2, C22, TS 2, TS 4, TS 7, and LP3K is shown at the left; for RCK106 (to K18) and for A45-B/B3, the reactivity was measured by incubating the blots with PUC-K18 before treating them with the antibodies. The reactivity with RCK106 therefore reflects the ability of the K8 fragments to "capture" the K18 fusion protein: (++) strong reactivity, (+) weak reactivity, and (−) no reactivity.

the antibody had a higher affinity for the K8−K18 complex than for individual polypeptides.

Epitope Analysis of A45-B/B3. Fourteen K8 fragments deleted progressively from the C-terminus were prepared by subcloning cDNA fragments into pGEX-2TE (see Figure 9) (*44*). Induction with 0.5 mM IPTG expressed these fragments as GST fusion proteins, which were detected by SDS−PAGE as the only major protein band in their respective bacterial lysate (Figure 10A). Predictably, the molecular mass of the fusion proteins was consistent with the size of the K8 inserts cloned in the pGEX. These fragments were used to determine the reactivity of different antibodies by Western blotting. To show that these fusion proteins contained K8 fragments, we probed the fusion proteins with LE41, an antibody with its epitope located closer to the head domain (residues 71−75) (*53*) that would react with most fragments. Consistent with this prediction, we observed reactivity of LE41 with 13 of the 14 K8 fragments (Figure 10B).

As mentioned above for the full-length K8, weak reactivity of A45-B/B3 with K8 fragments was observed only when the nitrocellulose membrane was blocked with 0.5% BSA and 0.5% Tween 20 in PBS. Blocking with 10% BSA or with 5−10% nonfat milk did not allow any reaction with the antibody (not shown). However, preincubation of the K8 fragments with a solution of PUC-K18 stimulated A45-B/B3 binding such that it could be detected even after the membrane was blocked with nonfat milk (Figure 10C). The smallest fragment of K8 reacting strongly with A45-B/B3 was K8CΔ151; the reactivity was reduced with K8CΔ161, and no reactivity was observed with K8CΔ171. Thus, the epitope of the antibody was located between residues 313 and 332, a stretch of 20 amino acids. However, as ∼20−30% of the immunoreactivity was retained in K8CΔ161, the high-affinity core epitope for surviving blotting was most likely located between residues 313 and 322.

To demonstrate that A45-B/B3 was reacting with the K8 polypeptide in the heterotypic complex, we incubated the K8 fragments bound to nitrocellulose with a solution of purified PUC-K18 and probed the membrane with RCK106, a K18 specific antibody. The smallest fragment that effectively captured K18 and produced a strong antibody binding signal was K8CΔ250, containing the head, coil 1A, linker L1, and coil 1B, which is ∼100 residues shorter than the smallest fragment that reacts with A45-B/B3 (see Figures 9 and 10). If A45-B/B3 were reacting with monomeric K18, then its reactivity profile would have been the same as that of RCK106, i.e., limited by the presence of K18 only (Figure 10C,D). This observation taken together with our ELISA data (Figure 8), therefore, strongly suggests that A45B/B3 does not react with a target on K18.

Using the same fragments, epitopes of a number of other anti-K8 monoclonal antibodies were similarly mapped. The binding results are shown in Figure 9. All the epitopes were located in the rod domain of the molecule except for the previously identified LE41 epitope (*53*). Seven of the monoclonal antibodies (CAM5.2, TROMA1, M20, NCL-5D3, RCK102, TS 1, and C22) recognized the same region, located between residues 353 and 367. The LP3K epitope was located close to the anti-IFA in the helix termination region. Besides reacting strongly with K8CΔ80, LP3K also exhibited significant reactivity with K8CΔ100, suggesting that the core epitope might lie between residues 368 and 383 but depends on sequences downstream (residues 384−403) for optimal folding to create a better fit epitope.

DISCUSSION

In this study, we have identified a region corresponding to residues 313−332 in the rod domain of human keratin K8 that is recognized by the A45-B/B3 monoclonal antibody, and we show that it plays a role in the stabilization of the keratin cytoskeleton. This antibody was originally raised in 1983 against keratin proteins present in MCF-7 cells and has been reported to react with K1/K2, K5, K8, and K18

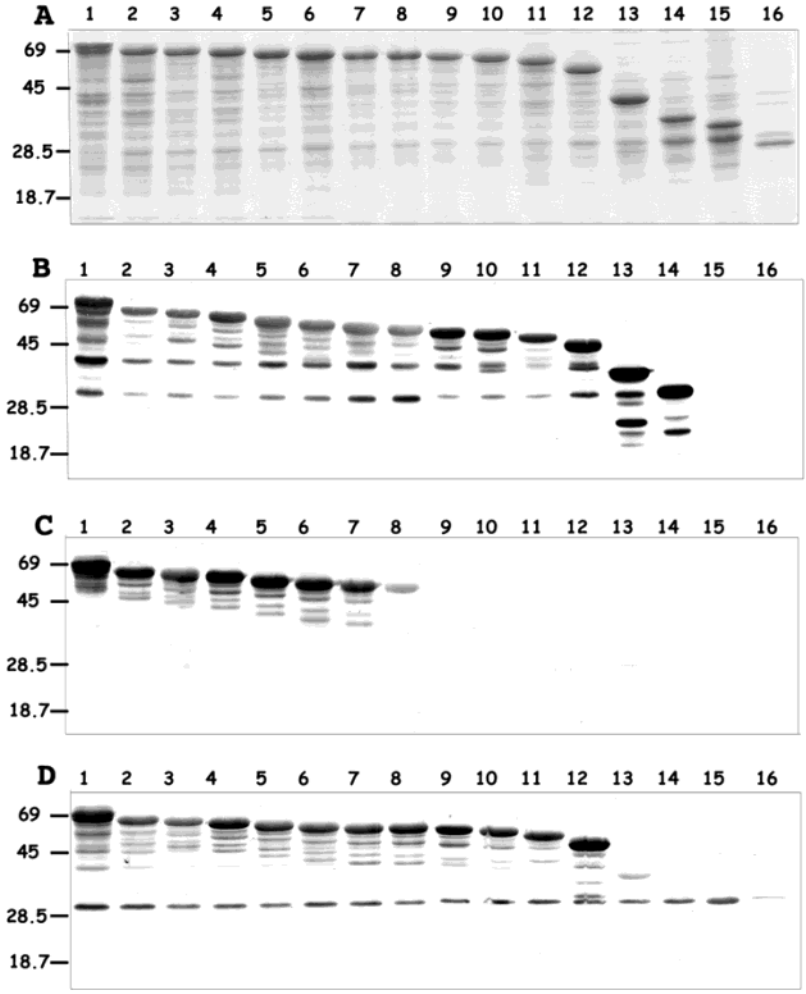

FIGURE 10: Western blotting of GST-K8 deletion fragments with antibodies. The 14 truncated K8 GST fusion protein fragments separated on a SDS gel and either visualized by Coomassie blue staining (A) or transferred onto nitrocellulose and reacted with LE41 followed by alkaline phosphatase-labeled goat anti-mouse antibody and visualized by NBT/BCIP reaction as described in Experimental Procedures (B). The GST-K8 fragments bound to a nitrocellulose membrane were incubated with a 20 μg/mL PUC-K18 (recombinant full-length K18 protein) solution in 4 M urea for 1 h and after washing with PBS reacted either with A45-B/B3 (C) or with RCK106 (D). The blots were developed as described for panel B: lane 1, GST-K8; lane 2, GST-K8CΔ80; lane 3, GST-K8CΔ100; lane 4, GST-K8CΔ116; lane 5, GST-K8CΔ131; lane 6, GST-K8CΔ141; lane 7, GST-K8CΔ151; lane 8, GST-K8CΔ161; lane 9, GST-K8CΔ171; lane 10, GST-K8CΔ184; lane 11, GST-K8CΔ218; lane 12, GST-K8CΔ250; lane 13, GST-K8CΔ354; lane 14, GST-K8CΔ398; lane 15, GST-K8CΔ417; and lane 16, GST.

(*54*). This antibody has been widely used in the identification of tumor cells in bone marrow smears from patients with breast (*55*), lung (*56*), esophagus (*57*), colon (*58*), and brain (*59*) cancers. A commercial kit (EPIMET) from Micromet AG (Munich, Germany) uses this antibody in carcinoma cell detection. Another carcinoma cell enrichment and detection kit from Miltenyi Biotec (Gladbach, Germany) employs CAM5.2, whose epitope has been characterized in this study. Defining specificities of such important reagents will have implications for understanding the basis for their selective reactivities with tumor cells. A45-B/B3 has been reported to react with K18 as determined by surface plasmon resonance, competitive ELISA, and immunoblotting assays (*60*). However, in our hands, A45-B/B3 reacted weakly with K8, reacted stronger with K8 and K18, and gave no specific reaction with either GST-K18 or PUC-K18. While the origin of this discrepancy between our results and those reported by others is not known, the improved antibody binding to K8 when K18 is present suggests that the preparations of K18 used in earlier studies might have been contaminated with K8 polypeptides. This premise is supported by the observation that A45-B/B3 was one of the very few antibodies tested in the earlier study to have reacted better with K8−K18 and K8−K19 complexes than with the individual keratins (*60*). Type I and type II keratin partners have very high affinity for each other, and it is notoriously difficult to completely separate them, which has led to misleading results in antibody characterization, e.g., CAM5.2 (*61*), which does not in fact react with K18 and K19 (*62*).

Previous studies have reported two different patterns of keratin aggregation induced by antibodies: (i) perinuclear coiling of filaments and (ii) keratin aggregation into globules (*40*, *41*). With A45-B/B3, we observed only keratin aggregates in 90% of injected cells, but occasionally perinuclear filament collapse was seen, with either the antibody or the Fab (see Figures 1, 5, and 6). These experiments were carried out over a period of a year or more with highly reproducible results, supporting the idea that this keratin disruption effect is specific to the antibody. The extent of antibody-induced disruption in different cell types was independent of the

number of keratins expressed; for example, HeLa and TR146 that expressed many more keratins than MCF-7 and BT20 (*8*) showed equally extensive disruption. The specificity of the reaction was shown by the fact that five of seven antibodies did not produce keratin aggregates. The induction of collapse of keratin filaments by the Fab fragment suggested that direct antibody binding, rather than cross-linking, causes the filament disruption. Furthermore, in PtK2 cells, where keratin filaments were only weakly stained with A45B/B3 (perhaps reflecting structural differences between the marsupial keratins and their human homologues), no collapse of filaments was induced by microinjection of this antibody. Taken together, these observations suggested that filament disruption required perturbation of molecular interactions in keratin filaments.

Previously, we have shown that monoclonal antibodies LE61 and LE65, which disrupt filaments (*39*, *52*), recognize complexes of K8 and K18 (*44*, *47*). However, there is a clear distinction between the LE61 and LE65 and A45-B/B3 epitopes, as LE61 and LE65 do not react alone but only react when the two polypeptides are associated together (*44*, *47*). It was therefore impossible to predict the contribution of individual polypeptides to reconstitution of the epitope. However, A45-B/B3 reacts with K8, albeit weakly, in ELISA and immunoblotting experiments. The dramatic increase in reactivity with a mixture of K8 and K18 suggests that a conformational change in K8, induced by interaction with K18, either makes the epitope more accessible or increases its affinity for the antibody. The antibody does not react directly with K18 in any of the assays used here (see Figures 8 and 10). The reactivity of A45-B/B3 was even greater with native keratins (extracted from MCF-7 cells) than with a mixture of PUC-K8 and PUC-K18, which could indicate the affinity of the antibody for a site of post-translational modification, absent in the recombinant keratins. Alternatively, the presence of K19 in MCF-7 cells would produce K8−K19 heterodimers, which may generate a higher-affinity epitope than K8−K18 dimers, resulting in an overall increase in the level of antibody binding. Further experiments using other keratins are required for a definitive explanation for this observation.

Several conformation specific keratin antibodies have been described in the literature, some reacting only under certain physiological conditions. Antibody KG8.13 only sees keratin filaments during mitosis (*63*), whereas others react with the pathological state; for example, AE1 and COU-1 react with neoplastic but not with normal cells (*64*, *65*), and M30 reacts with only K18 in the course of apoptosis (*66*). The ability of A45-B/B3 and RCK102 to identify the altered conformation of K8 in the heterotypic complex with K18 is unique, and a similar antibody has not been described. However, the inability of RCK102 to disrupt keratin filaments clearly distinguishes this antibody from A45-B/B3. Epitope analysis shows that the A45-B/B3 epitope is clearly distinct from the other K8 epitopes targeted by the antibodies examined here. This is consistent with these antibodies being unable to disrupt keratin filaments. Most of the epitopes that have been identified were located in coil 2B, which is consistent with the published observations (*60*); however, the locations of TS 7 and TS 1 epitopes are clearly different. Except for LE41, which was used as positive control, the rest of the epitopes have not been characterized before. Of the 14 antibodies that were mapped, seven were located between residues 353 and 367, suggesting that this is an immunodominant region (see Figure 11A).

Heterodimer formation is the first step on the path to filament assembly (*7*, *12*, *67*). Conformational changes that take place when keratin polypeptides associate into dimers and tetramers are largely unknown, although several indirect lines of evidence suggest that these changes are substantial. We have shown evidence that residues 313−332 in K8 adopt a different conformation on the transition from monomers or homodimers to heterodimers, as detected by binding of the A45-B/B3 antibody. The proteolytic instability of single keratins, as opposed to complementary pairs of keratins, also provides basic evidence for structural changes during heterotypic association (*6*, *68*). Furthermore, filament assembly using electron microscopy has shown formation of soluble unit-length filaments (ULFs) by association of tetramers. These ULFs, which are much thicker than normal filaments, associate longitudinally into loosely packed filaments and thereafter undergo compaction to reduce their thickness to 10 nm (*18*). This process clearly involves structural changes in individual subunits, consistent with the observation described here.

By comparing the target region sequence recognized by A45-B/B3 (Figure 11A) with others type II keratins and considering where these residues would lie in a dimeric α-helix (Figure 11B), one can see that the residues most likely contributing to the shared epitope are Arg, Arg, Glu, and Gln (residues in the *a* and *d* positions of the heptad repeat would be inaccessible to antibody in a dimer). These residues are not consecutive in the primary sequence but lie in a patch on the outside of the helical coil, within five turns of the helix (turns 1−3 and 5) in heptad positions *f*, *c*, *g*, and *g*, respectively. Thus, in a more relaxed configuration (in the monomeric or homodimeric form), the antibody may extend only over the Arg-Arg-Glu sequence, while if the K8 is packed in a tighter helix (as when combined with K18 in a dimer), the Gln might be brought sufficiently close to also contribute to a higher-affinity binding site. Circular dichroism spectroscopy suggested that mixing K8 and K18 produced a synergistic increase in α-helicity (unpublished results, R. A. Quinlan, personal communication) which would agree with our observations.

Disruption of keratin and vimentin filaments by the anti-IFA monoclonal antibody (*69*) is well-documented in the literature (*46*, *70*), and its epitope is located at the end of coil 2B (*71*, *72*), a critical region in filament assembly as indicated by several studies (*33*, *34*, *42*). The proximity of the LP3K epitope to that of anti-IFA would perhaps explain filament disruption by this antibody. The disruptive potential of A45-B/B3 suggests that its epitope should also lie in a site of association required for maintenance of stable filaments. Cross-linking data for keratin oligomers and filaments suggest stabilization of this region in keratins by extensive intermolecular interactions (*14*−*16*) which are likely to be influenced by antibody binding. A dynamic equilibrium between keratin filaments and a soluble pool of keratin intermediates has been demonstrated using microinjection of exogenous keratins (*26*−*28*) and by transfection of keratin cDNA constructs (*24*, *25*). It is, therefore, conceivable that binding of A45-B/B3 to a site vital for filament stabilization could lead to steric hindrance of the

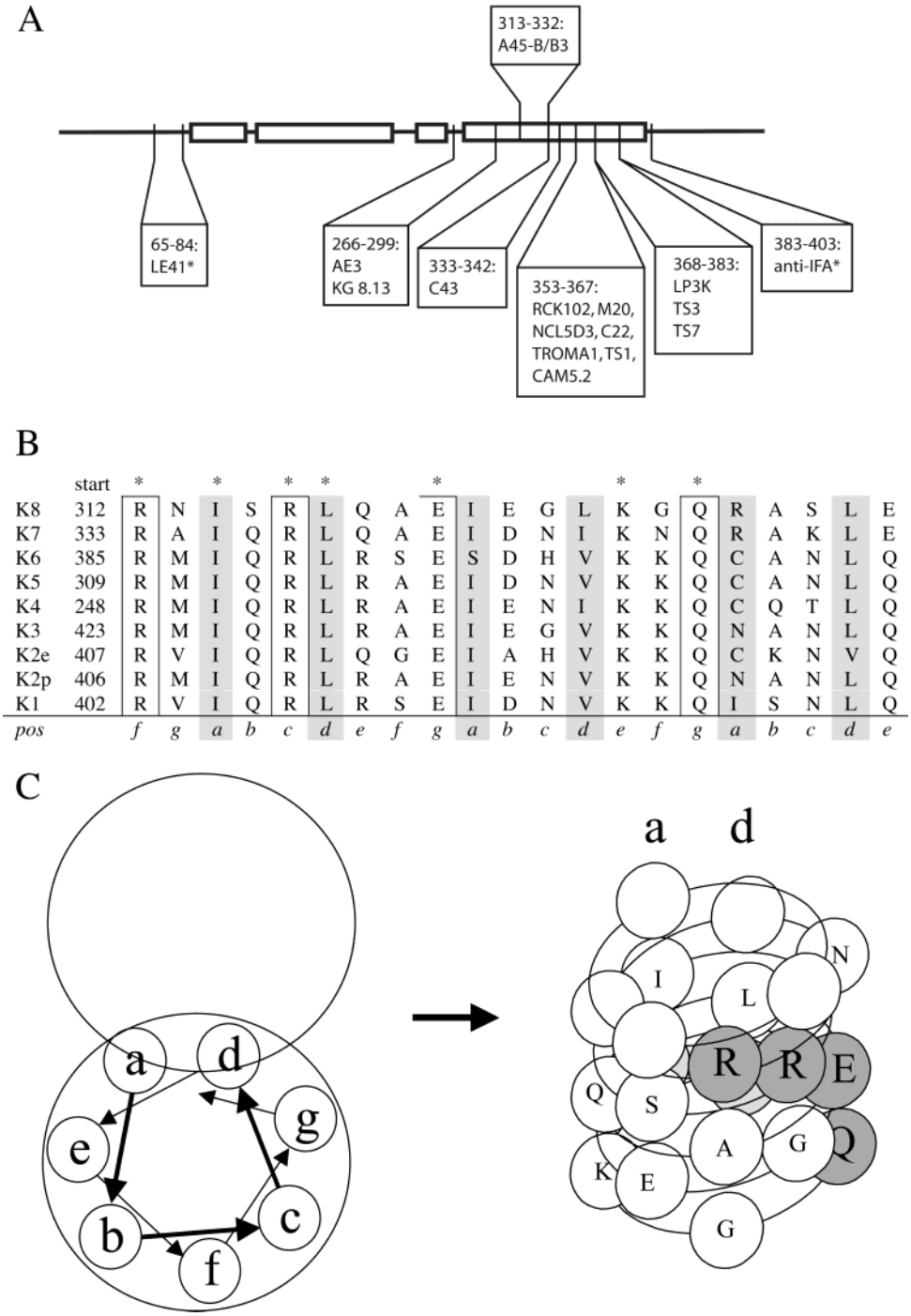

FIGURE 11: Localization of antibody epitopes on keratin K8. (A) The secondary structure of K8 is the same as depicted in Figure 9. The location of single keratin epitopes is given in boxes below, and the conformation-sensitive A45-B/B3 epitope is shown above. The numbers on the boxes signify the amino acids in the primary sequence defining the boundaries of the epitope region. Asterisks denote previously published work which indicates that the LE41 epitope is located between residues 71 and 75 (*53*) and that the anti-IFA epitope involves the last 10 amino acids of the rod domain (*42*). (B) Amino acid sequence across the A45-B/B3-recognized region as it appears in type II keratins 1−8, including the last residue of the previous fragment as this may be unfolded at an artificially free end of the truncated fragment. The "start" number identifies the position of the first residue in the overall keratin sequence (initiating methionine at position 1). Asterisks mark residues that are identical in all the keratins. Boxes indicate the residues most likely to contribute to the shared epitope; *Pos* (below) gives their respective heptad repeat positions from *a* to *g* (see panel C). (C) The packing of the seven-residue repeat through fewer than two helical turns, typical of proteins forming coiled coils, is shown end-on on the left. Positions *a* and *d* are occupied by hydrophobic or bulky residues and become sequestered at the interface between the two dimerizing polypeptides (as a leucine zipper); thus, *a* and *d* residues are unlikely to be accessible to antibody. A visualization of six turns (three heptads) is shown in a side view on the right. The four candidate residues, Arg, Arg, Glu, and Gln in positions *f*, *c*, *g*, and *g* over five turns (RREQ, shaded), would lie in a patch on the outer surface of the K8 α-helix. Dimerization with K18 may tighten the helix pitch to bring the four residues into a configuration of better fit for antibody binding.

K8/K18 interaction and could shift the equilibrium toward dissociation, thereby destabilizing the entire cytoskeleton. Whether the antibody-induced filament disruption involves dissociation into soluble intermediates or into keratin−

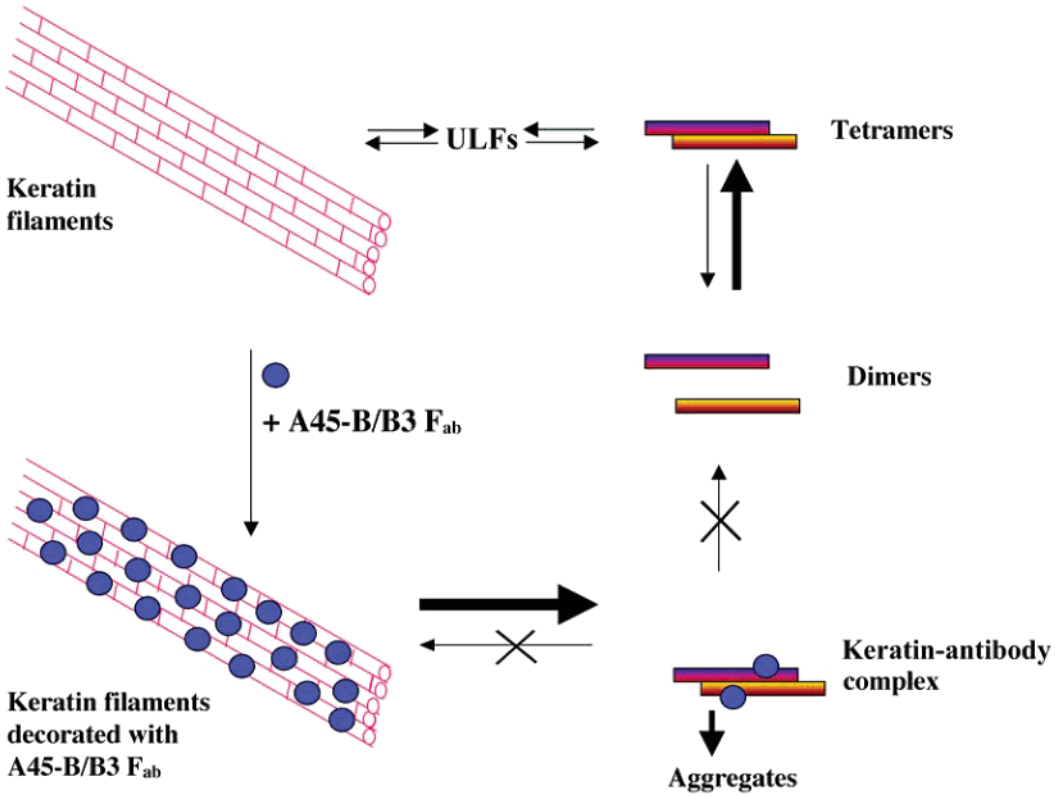

FIGURE 12: Possible mechanism of A45-B/B3-induced disruption of keratin filaments. The rapid equilibrium between keratin dimers and tetramers with a growing filament is disrupted by the introduction of A45-B/B3 or its Fab fragment. Initially, the keratin filaments are decorated by the Fab fragment, but with time, keratin filament−Fab complexes dissociate into aggregates which cannot reassociate with filaments. The absence of filament recovery for at least 24 h suggests these aggregates do not recycle into filaments, perhaps because of the high affinity of the Fab for keratin filaments. ULF represents unit-length filaments.

antibody aggregates is not clear. The fact that the aggregates remained in the cytoplasm for at least 24 h suggests that keratin polypeptides do not recycle into filaments after aggregation with the antibody (Figure 12).

In conclusion, we have shown that a 20-residue region in the rod domain of human keratin K8 is specifically recognized by A45-B/B3 and that the affinity of the antibody for this site increases significantly following dimerization with K18. This was observed using recombinant as well as naturally expressed keratins from MCF-7 cells. A number of other antibodies that were tested did not show significant differences in reactivity between the recombinant K8 and the MCF-7 keratins. The A45-B/B3 epitope is unique and does not overlap with 15 other antibody epitopes examined in this study. Microinjection of A45-B/B3 and its monovalent Fab fragment disrupted keratin filaments in several different epithelial cell lines, and this was not observed with other antibodies. Taken together, the data suggest that the A45-B/B3 epitope on human K8 is an important site for heterotypic association that probably undergoes a conformational change following interaction with keratin K18. Binding of the A45-B/B3 antibody or its Fab fragment to this site appears to influence the association−dissociation equilibrium and destabilize the cytoskeleton.

ACKNOWLEDGMENT

We are thankful to Jan Kovirak, Cynthia Dixon, Michael Klymkowsky, Torgny Stigbrand, Rolf Kemler, and David Lane for providing the monoclonal antibodies used in this study. We acknowledge the assistance of M. Kasper with the use of the immunofluorescence microscope and A. Ola, A. Lalli, and SeePaul Singh for technical help. We also acknowledge Joanne Stewart, Supriya Kapas, and Edward Odell for useful comments on the manuscript.

REFERENCES

1. Hesse, M., Magin, T. M., and Weber, K. (2001) *J. Cell Sci. 114*, 2569−2575.
2. Moll, R., Franke, W. W., Schiller, D. L., Geiger, B., and Krepler, R. (1982) *Cell 31*, 11−24.
3. Langbein, L., Rogers, M. A., Winter, H., Praetzel, S., Beckhaus, U., Rackwitz, H. R., and Schweizer, J. (1999) *J. Biol. Chem. 274*, 19874−19884.
4. Langbein, L., Rogers, M. A., Winter, H., Praetzel, S., and Schweizer, J. (2001) *J. Biol. Chem. 276*, 35123−35132.
5. Fuchs, E., and Weber, K. (1994) *Annu. Rev. Biochem. 63*, 345−382.
6. Kulesh, D. A., Cecena, G., Darmon, Y. M., Vasseur, M., and Oshima, R. G. (1989) *Mol. Cell. Biol. 9*, 1553−1565.
7. Hatzfeld, M., and Weber, K. (1990) *J. Cell Biol. 110*, 1199−1210.
8. Quinlan, R. A., Schiller, D. L., Hatzfeld, M., Achtstatter, T., Moll, R., Jorcano, J. L., Magin, T. M., and Franke, W. W. (1985) *Ann. N.Y. Acad. Sci. 455*, 282−306.
9. Purkis, P. E., Steel, J. B., Mackenzie, I. C., Nathrath, W. B., Leigh, I. M., and Lane, E. B. (1990) *J. Cell Sci. 97* (Part 1), 39−50.
10. Weber, K., and Geisler, N. (1985) *Ann. N.Y. Acad. Sci. 455*, 126−143.
11. North, A. C., Steinert, P. M., and Parry, D. A. (1994) *Proteins 20*, 174−184.
12. Steinert, P. M. (1990) *J. Biol. Chem. 265*, 8766−8774.
13. Geisler, N., Schunemann, J., and Weber, K. (1992) *Eur. J. Biochem. 206*, 841−852.
14. Steinert, P. M., Marekov, L. N., Fraser, R. D., and Parry, D. A. (1993) *J. Mol. Biol. 230*, 436−452.
15. Steinert, P. M., and Parry, D. A. (1993) *J. Biol. Chem. 268*, 2878−2887.

16. Steinert, P. M. (1993) *J. Invest. Dermatol. 100*, 729−734.
17. Parry, D. A., Marekov, L. N., and Steinert, P. M. (2001) *J. Biol. Chem. 276*, 39253−39258.
18. Herrmann, H., Wedig, T., Porter, R. M., Lane, E. B., and Aebi, U. (2002) *J. Struct. Biol. 137*, 82−96.
19. Lane, E. B., Goodman, S. L., and Trejdosiewicz, L. K. (1982) *EMBO J. 1*, 1365−1372.
20. Chou, Y. H., Bischoff, J. R., Beach, D., and Goldman, R. D. (1990) *Cell 62*, 1063−1071.
21. Horwitz, B., Kupfer, H., Eshar, Z., and Geiger, B. (1981) *Exp. Cell Res. 134*, 281−290.
22. Franke, W. W., Schmid, E., Mittnacht, S., Grund, C., and Jorcano, J. L. (1984) *Cell 36*, 813−825.
23. Magin, T. M., Bader, B. L., Freudenmann, M., and Franke, W. W. (1990) *Eur. J. Cell Biol. 53*, 333−348.
24. Albers, K., and Fuchs, E. (1987) *J. Cell Biol. 105*, 791−806.
25. Albers, K., and Fuchs, E. (1989) *J. Cell Biol. 108*, 1477−1493.
26. Miller, R. K., Vikstrom, K., and Goldman, R. D. (1991) *J. Cell Biol. 113*, 843−855.
27. Miller, R. K., Khuon, S., and Goldman, R. D. (1993) *J. Cell Biol. 122*, 123−135.
28. Vikstrom, K. L., Lim, S. S., Goldman, R. D., and Borisy, G. G. (1992) *J. Cell Biol. 118*, 121−129.
29. Okabe, S., Miyasaka, H., and Hirokawa, N. (1993) *J. Cell Biol. 121*, 375−386.
30. Angelides, K. J., Smith, K. E., and Takeda, M. (1989) *J. Cell Biol. 108*, 1495−1506.
31. Welch, W. J., and Suhan, J. P. (1986) *J. Cell Biol. 103*, 2035−2052.
32. Baribault, H., Blouin, R., Bourgon, L., and Marceau, N. (1989) *J. Cell Biol. 109*, 1665−1676.
33. Kouklis, P. D., Traub, P., and Georgatos, S. D. (1992) *J. Cell Sci. 102*, 31−41.
34. Hatzfeld, M., and Weber, K. (1992) *J. Cell Biol. 116*, 157−166.
35. Goldman, R. D., Khuon, S., Chou, Y. H., Opal, P., and Steinert, P. M. (1996) *J. Cell Biol. 134*, 971−983.
36. Birkenberger, L., and Ip, W. (1990) *J. Cell Biol. 111*, 2063−2075.
37. Papamarcaki, T., Kouklis, P. D., Kreis, T. E., and Georgatos, S. D. (1991) *J. Biol. Chem. 266*, 21247−21251.
38. Eckert, B. S., Daley, R. A., and Parysek, L. M. (1982) *Cold Spring Harbor Symp. Quant. Biol. 46* (Part 1), 403−412.
39. Klymkowsky, M. W., Miller, R. H., and Lane, E. B. (1983) *J. Cell Biol. 96*, 494−509.
40. Tolle, H. G., Weber, K., and Osborn, M. (1985) *Eur. J. Cell Biol. 38*, 234−244.
41. Boller, K., Kemler, R., Baribault, H., and Doetschman, T. (1987) *Eur. J. Cell Biol. 43*, 459−468.
42. Hatzfeld, M., and Weber, K. (1991) *J. Cell Sci. 99*, 351−362.
43. Wilson, A. K., Coulombe, P. A., and Fuchs, E. (1992) *J. Cell Biol. 119*, 401−414.
44. Waseem, A., Lane, E. B., Harrison, D., and Waseem, N. (1996) *Exp. Cell Res. 223*, 203−214.
45. Harlow, E., and Lane, D. P. (1998) *Using Antibodies: A Laboratory Manual*, Cold Spring Harbor Laboratory Press, Plainview, NY.
46. Klymkowsky, M. W. (1981) *Nature 291*, 249−251.
47. Waseem, A., White, K., and Waseem, N. H. (1997) *Int. J. Biochem. Cell Biol. 29*, 971−983.
48. Bottger, V., Stasiak, P. C., Harrison, D. L., Mellerick, D. M., and Lane, E. B. (1995) *Eur. J. Biochem. 231*, 475−485.
49. Waseem, A., Dogan, B., Tidman, N., Alam, Y., Purkis, P., Jackson, S., Lalli, A., Machesney, M., and Leigh, I. M. (1999) *J. Invest. Dermatol. 112*, 362−369.
50. Sambrook, J., Fritsch, E. F., and Maniatis, T. (1989) *Molecular Cloning: A Laboratory Manual*, Cold Spring Harbor Laboratory Press, Plainview, NY.
51. Bradford, M. M. (1976) *Anal. Biochem. 72*, 248−254.
52. Lane, E. B., and Klymkowsky, M. W. (1982) *Cold Spring Harbor Symp. Quant. Biol. 46* (Part 1), 387−402.
53. Bottger, V., and Lane, E. B. (1994) *J. Mol. Biol. 235*, 61−67.
54. Karsten, U., Widmaier, R., and Kunde, D. (1983) *Arch. Geschwulstforsch. 53*, 529−536.
55. Braun, S., Pantel, K., Muller, P., Janni, W., Hepp, F., Kentenich, C. R., Gastroph, S., Wischnik, A., Dimpfl, T., Kindermann, G., Riethmuller, G., and Schlimok, G. (2000) *N. Engl. J. Med. 342*, 525−533.
56. Offner, S., Schmaus, W., Witter, K., Baretton, G. B., Schlimok, G., Passlick, B., Riethmuller, G., and Pantel, K. (1999) *Proc. Natl. Acad. Sci. U.S.A. 96*, 6942−6946.
57. Thorban, S., Rosenberg, R., Busch, R., and Roder, R. J. (2000) *Br. J. Cancer 83*, 35−39.
58. Leinung, S., Wurl, P., Weiss, C. L., Roder, I., and Schonfelder, M. (2000) *Langenbecks Arch. Surg. 385*, 337−343.
59. Maguire, D., O'Sullivan, G. C., McNamara, B., Collins, J. K., and Shanahan, F. (2000) *Qjm 93*, 611−615.
60. Stigbrand, T., Andres, C., Bellanger, L., Bishr Omary, M., Bodenmuller, H., Bonfrer, H., Brundell, J., Einarsson, R., Erlandsson, A., Johansson, A., Leca, J. F., Levi, M., Meier, T., Nap, M., Nustad, K., Seguin, P., Sjodin, A., Sundstrom, B., van Dalen, A., Wiebelhaus, E., Wiklund, B., Arlestig, L., and Hilgers, J. (1998) *Tumor Biol. 19*, 132−152.
61. Makin, C. A., Bobrow, L. G., and Bodmer, W. F. (1984) *J. Clin. Pathol. 37*, 975−983.
62. Smedts, F., Ramaekers, F. C. S., Robben, H., Pruszczynski, M., van Muijen, G., Lane, B., Leigh, I., and Vooijs, P. (1990) *Am. J. Pathol. 136*, 657−668.
63. Franke, W. W., Winter, S., Schmid, E., Sollner, P., Hammerling, G., and Achtstatter, T. (1987) *Exp. Cell Res. 173*, 17−37.
64. Asch, B. B., and Asch, H. L. (1986) *Cancer Res. 46*, 1255−1262.
65. Ditzel, H. J., Strik, M. C., Larsen, M. K., Willis, A. C., Waseem, A., Kejling, K., and Jensenius, J. C. (2002) *J. Biol. Chem. 277*, 21712−21722.
66. Leers, M. P., Kolgen, W., Bjorklund, V., Bergman, T., Tribbick, G., Persson, B., Bjorklund, P., Ramaekers, F. C., Bjorklund, B., Nap, M., Jornvall, H., and Schutte, B. (1999) *J. Pathol. 187*, 567−572.
67. Hatzfeld, M., Maier, G., and Franke, W. W. (1987) *J. Mol. Biol. 197*, 237−255.
68. Lu, X., and Lane, E. B. (1990) *Cell 62*, 681−696.
69. Pruss, R. M., Mirsky, R., Raff, M. C., Thorpe, R., Dowding, A. J., and Anderton, B. H. (1981) *Cell 27*, 419−428.
70. Meyer, T., Weber, K., and Osborn, M. (1992) *Eur. J. Cell Biol. 57*, 75−87.
71. Geisler, N., Kaufmann, E., Fischer, S., Plessmann, U., and Weber, K. (1983) *EMBO J. 2*, 1295−1302.
72. Magin, T. M., Hatzfeld, M., and Franke, W. W. (1987) *EMBO J. 6*, 2607−2615.
73. Lane, E. B. (1982) *J. Cell Biol. 92*, 665−673.
74. Schaafsma, H. E., Ramaekers, F. C., van Muijen, G. N., Lane, E. B., Leigh, I. M., Robben, H., Huijsmans, A., Ooms, E. C., and Ruiter, D. J. (1990) *Am. J. Pathol. 136*, 329−343.
75. Angus, B., Purvis, J., Stock, D., Westley, B. R., Samson, A. C., Routledge, E. G., Carpenter, F. H., and Horne, C. H. (1987) *J. Pathol. 153*, 377−384.
76. Bartek, J., Vojtesek, B., Staskova, Z., Bartkova, J., Kerekes, Z., Rejthar, A., and Kovarik, J. (1991) *J. Pathol. 164*, 215−224.
77. Sundstrom, B. E., Nathrath, W. B., and Stigbrand, T. I. (1989) *J. Histochem. Cytochem. 37*, 1845−1854.
78. Kemler, R., Brulet, P., Schnebelen, M. T., Gaillard, J., and Jacob, F. (1981) *J. Embryol. Exp. Morphol. 64*, 45−60.
79. Lane, E. B., Bartek, J., Purkis, P. E., and Leigh, I. M. (1985) *Ann. N.Y. Acad. Sci. 455*, 241−258.
80. Ramaekers, F., Huysmans, A., Schaart, G., Moesker, O., and Vooijs, P. (1987) *Exp. Cell Res. 170*, 235−249.
81. Gigi, O., Geiger, B., Eshhar, Z., Moll, R., Schmid, E., Winter, S., Schiller, D. L., and Franke, W. W. (1982) *EMBO J. 1*, 1429−1437.
82. Woodcock-Mitchell, J., Eichner, R., Nelson, W. G., and Sun, T. T. (1982) *J. Cell Biol. 95*, 580−588.
83. Ramaekers, F. C., Moesker, O., Huysmans, A., Schaart, G., Westerhof, G., Wagenaar, S. S., Herman, C. J., and Vooijs, G. P. (1985) *Ann. N.Y. Acad. Sci. 455*, 614−634.
84. Ramaekers, F., Huysmans, A., Moesker, O., Kant, A., Jap, P., Herman, C., and Vooijs, P. (1983) *Lab. Invest. 49*, 353−361.

BI035072S